Cellulose (2013) 20:1031–1040
DOI 10.1007/s10570-013-9899-1

ORIGINAL PAPER

Small-angle scattering study of structural changes in the microfibril network of nanocellulose during enzymatic hydrolysis

Paavo A. Penttilä · Anikó Várnai · Manuel Fernández · Inkeri Kontro · Ville Liljeström · Peter Lindner · Matti Siika-aho · Liisa Viikari · Ritva Serimaa

Received: 11 January 2013 / Accepted: 4 March 2013 / Published online: 12 March 2013

Abstract The hydrolysis of nanofibrillated cellulose (NFC), consisting of individual cellulose fibrils, was followed using small-angle scattering techniques in order to reveal changes in the substrate structure caused by cellulose degrading enzymes. In particular, the nanoscale structure of the network of cellulose fibrils was characterized with the combination of small-angle neutron scattering and small-angle x-ray scattering. In the nanocellulose with higher xylan content, the interfibrillar distance was shown to remain unchanged during enzymatic degradation, whereas the distance increased in the nanocellulose with lower xylan content. The limiting effect of xylan on the hydrolysis and a faster hydrolysis of the more thoroughly fibrillated segments of the NFC network could be observed. Despite the extensive fibrillation of the raw material, however, the hydrolysis was eventually limited by the aggregated and heterogeneous structure of the substrate.

Keywords Enzymatic hydrolysis · Bioethanol · Cellulose · Hemicellulose · SANS · SAXS

P. A. Penttilä (✉) · I. Kontro · V. Liljeström · R. Serimaa
Department of Physics, University of Helsinki, P.O. Box 64, 00014 Helsinki, Finland
e-mail: paavo.a.penttila@helsinki.fi

A. Várnai · L. Viikari
Department of Food and Environmental Sciences, University of Helsinki, P.O. Box 27, 00014 Helsinki, Finland

M. Fernández
ID02, European Synchrotron Radiation Facility (ESRF), 6 Rue Jules Horowitz, B.P. 220, 38043 Grenoble, France

P. Lindner
D11, Institut Laue-Langevin (ILL), 6 Rue Jules Horowitz, B.P. 156, 38042 Grenoble, France

M. Siika-aho
VTT Technical Research Centre of Finland, P.O. Box 1000, 02044 Espoo, Finland

Introduction

Utilization of non-food biomass represents a highly potential option as a response to the growing demand for renewable and sustainable fuels. Despite serious efforts made in order to overcome the natural recalcitrance of biomass, the inefficiency of enzymatic hydrolysis still remains as one of the key challenges in the conversion of biomass to fermentable sugars (Chundawat et al. 2011). The recalcitrance of biomass is primarily caused by its highly hierarchical ordered structure which limits the accessibility of enzymes to the bulk of cellulose (Arantes and Saddler 2010; Penttilä et al. 2010). Thus, prior to enzymatic hydrolysis, the recalcitrant structure of biomass needs to be modified with pretreatment (Chundawat et al. 2011). Yet, our current understanding on the mechanisms of different pretreatment methods and of the enzymatic action on lignocellulose is incomplete

(Chundawat et al. 2011). The main structural features limiting enzymatic hydrolysis have been specified in literature as high crystallinity, small accessible surface area as well as hemicellulose and lignin content (Alvira et al. 2010; Hallac and Ragauskas 2011; Penttilä et al. 2013; Zhu et al. 2008). In the hydrolysis of lignocellulose, however, these limiting factors are closely interconnected. Therefore, simplified hydrolytic systems would be necessary to separately model factors structurally limiting enzymatic hydrolysis.

The aggregation of cellulose microfibrils limits the accessibility of enzymes and hence the physical breakdown of microfibrillar aggregates is necessary to allow enzymatic action on a network of separated fibrils. Mechanical fibrillation of chemical pulp produces nanofibrillated cellulose (NFC), in which the elementary microfibrils are separated from each other and form a three-dimensional network with a high capacity for water adsorption. In nanofibrillated cellulose, the majority of fibrils are separated and hence directly accessible by enzymes, which enables the study of enzymatic hydrolysis without limitations caused by the aggregation of the fibrils.

Besides the aggregation of cellulosic microfibrils, the presence of hemicellulose is known to hinder the enzymatic hydrolysis of cellulose. Recently, xylan has been found to impede the enzymatic degradation of NFC produced from hardwood chemical pulp and has been shown to affect the hydrolysis of cellulose crystals in particular (Penttilä et al. 2013). The exact location of xylan in lignocellulosic biomass and the mechanism how xylan limits the enzymatic hydrolysis of cellulose on a larger length scale, i.e. in the network structure of NFC, is still unclear. The limiting role of xylan could be studied when partially removing xylan from lignocellulose with purified xylanases.

Nanoscale structural changes take place in biomass during enzymatic hydrolysis, which may have an impact on the enzyme accessibility and cellulose digestibility (Santa-Maria and Jeoh 2010; Wang et al. 2006; Zhou et al. 2009). The size and shape of nanometer-sized pores between the fibril aggregates in cellulosic biomass, determining a large proportion of the available surface area, is altered continuously due to the action of enzymes (Penttilä et al. 2010; Kent et al. 2010). The enlargement of pores has been attributed to the peeling mechanism of enzymatic hydrolysis as only the outermost fibrils on the pore surface are exposed to the enzymes (Penttilä et al. 2010; Kent et al. 2010). According to recent findings using time-resolved atomic force microscopy (AFM) techniques, the degradation of the pore surface seems to proceed heterogeneously, aided by crack formation (Bubner et al. 2012). Although the enlargement of pores helps enzymes approach previously unavailable surfaces, the pore surface becomes rougher and the length of the obstacle-free ways for the processive cellobiohydrolase (CBH) enzymes are reduced. As a consequence, the CBH enzymes are not able to proceed along the surface and they will get jammed (Igarashi et al. 2011; Jalak and Väljamäe 2010). On the other hand, also non-processive endoglucanases (EG) may get trapped in physical structures (Murphy et al. 2012).

Small-angle x-ray scattering (SAXS) and small-angle neutron scattering (SANS) have been successfully used in studying the hierarchical structure of lignocellulosic biomaterials at nanoscale and changes in structure during enzymatic hydrolysis (Penttilä et al. 2010; Kent et al. 2010). The advantage of using small-angle scattering methods is that they are non-destructive and that the relatively large sample volume enables the observation of a representative amount of sample despite dilute dispersion. The possibility of contrast variation achieved by varying the D_2O/H_2O ratio of the solvent, makes SANS especially attractive to overcome the relatively low scattering length density contrast of both x-rays and neutrons between cellulose and water (Lopez-Rubio and Gilbert 2009; Shibayama 2011). Replacing water with deuterated water in never-dried cellulosic dispersions is challenging and needs to be carried out without drying the samples in order to prevent irreversible structural changes such as nanoscale aggregation of cellulose microfibrils (Penttilä et al. 2010).

In this work, the structural limitations of the enzymatic hydrolysis of holocellulosic biomass were studied by hydrolysing nanofibrillated cellulose samples having varying xylan contents. Changes in the polymeric network structure, formed by individual cellulose fibrils, were followed using small-angle scattering methods, SANS and SAXS, without drying the samples.

Materials and methods

Materials

Nanocellulose with different xylan contents was prepared from bleached birch kraft pulp and

hydrolysed to various extents with commercial enzyme mixture as described previously by Penttilä et al. (2013). In short, birch wood chemical pulp was digested with xylanase to produce pulp with reduced xylan content. The original and the xylanase digested pulps were mechanically fibrillated to obtain nanofibrillated cellulose (NFC) with high (HX) and low xylan content (LX), respectively. These substrates were then hydrolysed for varying durations, resulting in residues hydrolysed to varying degrees (Table 1). After the hydrolysis, the bound enzymes were cleaved by protease and the small water-soluble molecules were removed by dialysis (Penttilä et al. 2013). The samples were concentrated to a dry matter content of around 1 %.

In the aqueous dispersion of the nanocellulosic materials (substrates and hydrolysis residues), water was replaced with D_2O/H_2O mixture in ratios of 1:0, 2:1, 1:2, and 0:1 (later referred to as 100 % D_2O, 67 % D_2O, 33 % D_2O, and 0 % D_2O, respectively) in consecutive concentration–dilution steps. The samples were first concentrated to a volume of approximately 15 to 25 % of the original with centrifugal ultrafiltration (VIVASPIN 4, membrane cut-off 5 kDa, Sartorius Stedim; 8,300 rpm at 16 °C), then re-diluted with D_2O/H_2O mixture. The procedure was repeated two more times, after which the samples were equilibrated in room temperature for 12 to 66 h before SANS measurements. The same samples were used later in the SAXS experiments.

Table 1 Properties of the hydrolysis residues (Penttilä et al. 2013)

Sample	Anhydro-sugar composition (wt%)[a]		Hydrolysis degree (%)[b]
	Glucose	Xylose	
HX[c]	76	24	–
HX[c] 25 %	73	27	23
HX[c] 50 %	67	33	48
HX[c] 75 %	53	47	72
LX[d]	88	12	–
LX[d] 25 %	87	13	25
LX[d] 50 %	87	13	47
LX[d] 75 %	84	16	78

[a] Composition based on the ratio of glucose and xylose detected by HPLC from the substrate (HX/LX) or hydrolysate (HX/LX 25 %, HX/LX 50 %, HX/LX 75 %)

[b] Total yield of glucose and xylose relative to the original substrate mass

[c] High xylan content

[d] Low xylan content

Small-angle neutron scattering

The measurements were carried out at the SANS instrument D11 of ILL in Grenoble, France. Three positions of the He gas detector (1.2 m, 8.0 m and 39.0 m, with collimation distances 8.0, 8.0 and 40.5 m) were used to cover a range of 0.0014–0.52 $Å^{-1}$ for the magnitude of the scattering vector

$$q = \frac{4\pi \sin\theta}{\lambda} \quad (1)$$

with wavelength $\lambda = 6$ Å and θ defined as half of the scattering angle. The samples were measured in quartz cells (Hellma) with a sample path length of 1 mm and volume of 700 µl. The temperature of the sample holder was adjusted to 12 °C and the diameter of the circular neutron-beam cross-section was 10 mm. The samples were measured for 2 and 15 min at detector positions 1.2 and 8 m, whereas the measuring time for the longest distance varied between 60 and 120 min. The transmitted intensity of each sample was measured with the beamstop removed and using an attenuator to protect the detector.

The two-dimensional scattering patterns were integrated and converted to absolute scale (here the word 'intensity' is used for the differential scattering cross section, unit cm^{-1}) using the Large Array Manipulation Program (LAMP) software (http://www.ill.eu/data_treat/lamp/the-lamp-book) and H_2O as (secondary) standard (Lindner 2002). The corrected intensity as a function of q is thus

$$I_s^{corr}(q) = \frac{I'_s(q) \cdot [1/(t_s N_s)]}{I'_w(q) \cdot [1/(t_w N_w)]} \cdot \left(\frac{\chi_{H_2O}}{F_{sc}}\right), \quad (2)$$

where $I'_s(q)$ and $I'_w(q)$ are the measured intensities of sample and water, respectively, corrected for losses due to dead-time of the detector, q dependence of the attenuation, efficiency of each detector pixel, scattering of an empty cell, electronic noise of the detector (from an absorbent measurement with a cadmium sheet), transmission of an empty cell and intensity decrease as a function of q due to solid angle. The variables t_s and t_w represent the counting times and N_s and N_w the monitor counts for sample and water, respectively. The instrument-specific effective

differential scattering cross section of water χ_{H_2O} was determined earlier with a polymer standard and the scaling factor F_{sc} was 0.00164 for detector distance 39 m and 1.0 for the other distances, for which H_2O was measured separately. The corrected intensity of the corresponding solvent was subtracted from the scattering intensity of each sample afterwards.

Small-angle x-ray scattering

SAXS was measured for the non-hydrolysed and the 50 % hydrolysed NFC samples at the ID02 beam line of ESRF in Grenoble, France. The measurements were conducted using a pinhole camera, where a premonochromatized (12.46 keV or $\lambda = 0.995$ Å) pencil-beam was shaped with slits to be 300 µm × 300 µm in cross-section. The scattered radiation was recorded using a two-dimensional FReLoN Kodak CCD detector at distances of 1.0 and 10.0 m. The SAXS scattering patterns were normalized to the absolute intensity and corrected by the transmission of the sample using SAXS Utilities software (http://www.sztucki.de/SAXSutilities). Data measured at different detector distances were combined, yielding a q range of 0.0010–0.051 $Å^{-1}$ in total. The scattering vector was defined from the pinhole setup geometry, using Eq. 1. The effective total exposure time was of about 100 ms, taking care to avoid radiation damage to the sample.

The wet samples were placed in sealed glass capillaries with a diameter of 1 mm. The drying sample (few microliters) was set on adhesive tape placed vertically, perpendicular to the beam. The viscosity of the sample prevented the drop from sliding down. Since the thickness of the sample changed with time, a normalization with the transmission was performed for every scattering pattern.

Results and discussion

General features of the scattering intensities

Small-angle scattering methods, SANS and SAXS, were applied to enzymatically hydrolysed nanocellulose in order to reveal changes in the network structure of fibrillated cellulose during the hydrolysis. The SANS and SAXS intensity profiles (Figs. 1 and 2) corresponded well to each other on the overlapping q range 0.0014–0.051 $Å^{-1}$ (Fig. 2). When water was completely replaced with deuterated water (100 % D_2O), the features of the SANS intensities at larger q values became more pronounced due to the higher

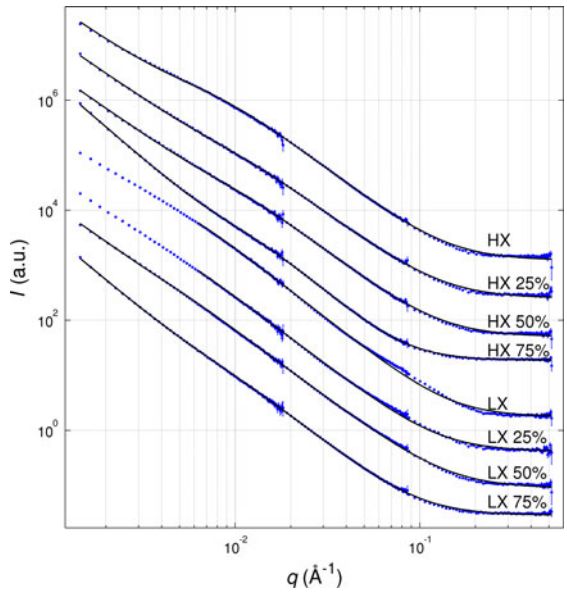

Fig. 1 Measured SANS intensities from enzymatically hydrolysed nanocellulose in 100 % D_2O solution (*dots with error bars* based on counting statistics) and fits of Eq. 3 to the experimental data (*solid lines*), shifted vertically for clarity

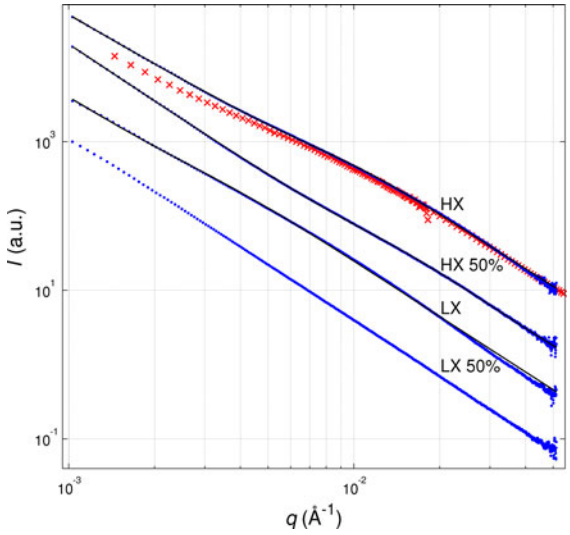

Fig. 2 Measured SAXS intensities from enzymatically hydrolysed nanocellulose (*dots*) and fits of Eq. 3 to the experimental data (*solid lines*), shifted vertically for clarity. Scaled SANS intensity of sample HX in 100 % D_2O is plotted with crosses for comparison on the common q range

scattering length density contrast between cellulose and the solvent, as compared to that of cellulose and water in SAXS (Fig. 2).

The SANS intensity profiles of most samples in 100 % D_2O solution (Fig. 1) showed a shoulder-like form, which also appeared, although less pronounced, on the SAXS intensity profiles (Fig. 2). In the HX samples this shoulder could be located around $q = 0.012$ Å^{-1}, which corresponds to the Bragg distance of about 50 nm. In the non-hydrolysed LX sample, a similar feature could be detected at smaller q values, around $q = 0.004$ Å^{-1}, whereas in the hydrolysed LX samples, the shoulder was hardly detectable. In fact, the most hydrolysed LX samples (LX 50 % and LX 75 %) displayed a weaker shoulder located on larger q values, similar to that of the HX samples. Based on the length scale of the Bragg distances corresponding to their locations and findings of other SAXS studies (Kennedy et al. 2007; Leppänen et al. 2009), the shoulder features were predicted to arise from the interfibrillar repeating distance in the NFC network and they would thus be characteristic of the mesh size of the network. To support this interpretation, a SAXS experiment was performed on a sample of non-hydrolysed HX, which was dried during the measurement in order to collapse its three-dimensional structure. The scattering intensities of this sample (Fig. 3) showed a clear shift of the peak (on (q, q^2I) scale, i.e. Kratky plot) from a Bragg distance of around 50 nm to below 30 nm during drying. Thus, as

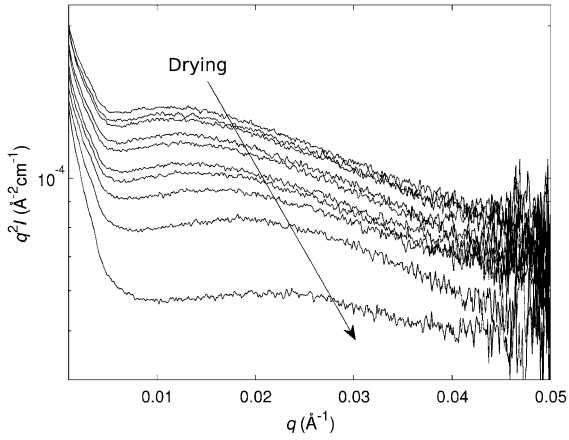

Fig. 3 SAXS Kratky plot of a drying NFC sample (HX), starting at 20 min after the beginning of the drying and measured at 3 min intervals. The peak related to the interfibrillar distance is shifted towards larger q values

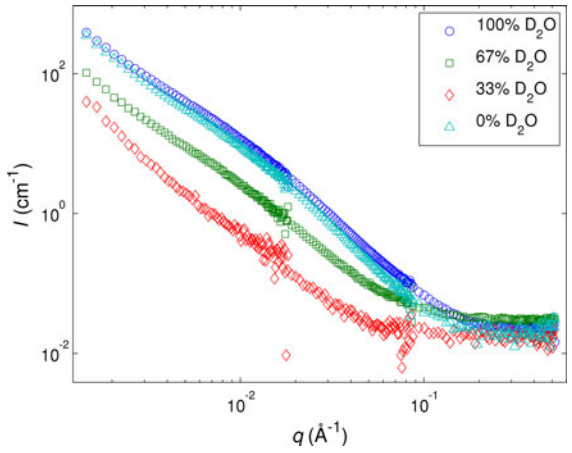

Fig. 4 Contrast variation of non-hydrolysed HX measured with SANS

the drop of NFC dried and water was removed from the interfibrillar space, the distance between neighboring fibrils was reduced. In addition, the shoulder disappeared when the scattering length density contrast was reduced by changing the D_2O/H_2O ratio in the solvent (Fig. 4), proving that the feature arose from the contrast between cellulose fibrils and the surrounding solvent.

Fractal dimensions from power law fits

To quantify the shape of the scattering curves, power laws of the form $I(q) \sim q^{-D}$ were fitted to the experimental SANS and SAXS data on regions mostly consisting of q values below the shoulder (Table 2). The regions were chosen visually, causing an estimated error in the order of ±0.01 to the value of D. The power D can be interpreted as the mass fractal dimension of the structures in the corresponding length scale (roughly 100–500 nm) (Penttilä et al. 2010). All values of D in Table 2 were found to be between 1.9 and 2.8 with both SANS and SAXS, and corresponded to a fairly loose structure (Penttilä et al. 2010) which describes adequately a network of cellulose fibrils in NFC. The fractal dimension increased during hydrolysis, which suggests a slight densification of the structure. However, the increasing trend seems to be partly caused by the weakening of the shoulder, as the low-q tail of the shoulder directly affected the power law fit especially in the HX samples.

Table 2 Parameters from power law fits ($I(q) \sim q^{-D}$) to SANS (100 % D_2O) and SAXS Data

	SANS			SAXS		
	q_{min} (Å^{-1})	q_{max} (Å^{-1})	D	q_{min} (Å^{-1})	q_{max} (Å^{-1})	D
HX	0.0014	0.0030	1.9	0.0010	0.0035	2.2
HX 25 %	0.0014	0.0038	2.3	–	–	–
HX 50 %	0.0014	0.0140	2.1	0.0010	0.0045	2.5
HX 75 %	0.0014	0.0050	2.8	–	–	–
LX	0.0014	0.0063	2.0	0.0010	0.0060	2.1
LX 25 %	0.0014	0.0070	2.2	–	–	–
LX 50 %	0.0014	0.0140	2.3	0.0010	0.014	2.5
LX 75 %	0.0014	0.0050	2.7	–	–	–

Empirical network model

In order to consider the power law behavior and the shoulder in a single fit, and to characterize the network structure of NFC more quantitatively, the SANS and SAXS data were fitted with a function of the form

$$I(q) = \frac{A}{q^n} + \frac{C}{1 + (\xi q)^m} + B, \quad (3)$$

which is an empirical model used for polymer solutions and randomly cross-linked hydrogels (Horkay and Hammouda 2008; Waters et al. 2011). In Eq. 3, the first term corresponds to the pure power law or Porod type behavior of the scattering intensity and the second term characterizes the fibril network, with ξ referred to as the correlation length. The parameters n and m are power law exponents independent of each other, A and C are scaling constants, and B accounts for a constant background. All these parameters, including ξ, were kept floating in the fits. Weighted non-linear least-squares fits were performed on the full experimental q range for all measured intensities except for the SANS data of samples LX and LX 25 %, for which the first term of the fitting function in Eq. 3 was omitted and the region of the fit was manually chosen to begin at $q = 0.0063$ Å^{-1}. In fits to SANS data, the data points were weighted by the reciprocals of the statistical errors of individual data points (error bars in Fig. 1), whereas in the case of SAXS data, the reciprocal of the square root of the number of counts was used to weight each data point. The SAXS intensity of sample LX 50 % could not be fitted with Eq. 3 at all, because it displayed too dominant power law behavior (Fig. 2). The goodness of each fit was characterized by calculating the coefficient of determination R^2 (Table 3).

Changes in the network structure due to enzymatic hydrolysis

As with the power laws, the fits of Eq. 3 gave congruent values for the optimal fitting parameters for the SANS and SAXS data (Table 3). The parameter responsible for the pure power law behavior, n, had similar values as the power law exponent D on lower q values (Table 2), increasing from around 2.3 to 2.8 or 2.9 by hydrolysing 75 % of the theoretical maximum yield in both sample series. At lower conversions, the increment of this parameter was only minor. If interpreted based on the fractal model (Penttilä et al. 2010), this would indicate a densified structure of the fibrillar network in the 75 % hydrolysed samples. On the other hand, the increased intensity at lower q values may be due to a greater proportion of larger structures accumulating during the extensive hydrolysis. The exponent m in the second term in Eq. 3 did not show systematic behavior (Table 3), which may be explained by the lower contribution of the second term to the overall scattering in many samples.

The correlation length ξ, previously used to describe the mesh size of a polymer network (Horkay and Hammouda 2008; Waters et al. 2011), seemed to be closely connected with the shoulder features of the scattering intensities, which became more evident when the intensity was multiplied by the square of the scattering vector (Figs. 5 and 6). Therefore, this parameter was predicted to describe the interfibrillar distance in the NFC network. Even though the values obtained for the correlation length ξ (7–38 nm) were smaller than expected for a loose network of fibrils, fits made to the SAXS intensities of the drying non-hydrolysed HX sample (Fig. 3) using the empirical network model showed a gradual decrease in the correlation length ξ from 6 to 4 nm (data not shown). The values were well in agreement with the value of 4.0 nm determined earlier for the width of the cellulose crystallites (Penttilä et al. 2013). While the correlation length might not correspond to any exact monodisperse distance between the fibrils, it certainly reflects the interfibrillar distance in the samples.

When examining the SANS Kratky plots of the HX sample series (Fig. 5a) in more detail, it could be seen

Table 3 Parameters from fits of Eq. 3 to SANS (100 % D_2O) and SAXS Data

Sample	SANS						SAXS					
	A (10^{-5} cm^{-1})	n	C (cm^{-1})	ξ (nm)	m	R^2	A (10^{-5} cm^{-1})	n	C (cm^{-1})	ξ (nm)	m	R^2
HX	8.68	2.35	22.6	12.8	2.59	0.996	10.1	2.23	3.43	9.72	2.96	1.000
HX 25 %	13.2	2.32	5.71	9.87	2.61	0.997	–	–	–	–	–	–
HX 50 %	12.6	2.35	5.88	9.37	2.78	0.999	1.85	2.55	1.05	7.02	2.99	1.000
HX 75 %	0.886	2.91	7.09	8.54	2.83	0.998	–	–	–	–	–	–
LX	–	–	427	27.9	2.63	0.999	7.10	2.38	39.3	28.1	2.76	0.999
LX 25 %	–	–	317	37.5	2.54	0.999	–	–	–	–	–	–
LX 50 %	16.8	2.40	18.7	18.4	3.05	0.999	–	–	–	–	–	–
LX 75 %	1.43	2.81	11.8	13.3	2.46	0.998	–	–	–	–	–	–

that the position of the peak remained approximately constant (at about $q = 0.011$ Å^{-1}), whereas its intensity was weakened during the hydrolysis. Also the correlation length ξ decreased slightly, from 13 to 9 nm based on the fits of the empirical network model to the SANS intensities (Eq. 3, Table 3). Due to the weakening of the peak in Fig. 5a, the contribution of the interfibrillar correlation term (second term in Eq. 3) to the fit was decreased, which was demonstrated by calculating the area below this term relative to the area below the whole fit. The obtained ratios were 0.31, 0.10, 0.10, and 0.07 for the samples HX, HX 25 %, HX 50 %, and HX 75 %, respectively. Thus, as the contribution of the correlation shoulder (second term in Eq. 3) decreased with the increasing conversion yields, the power law behavior of the intensity (first term in Eq. 3), originating from larger structures, started to dominate the intensity profile. These results indicate that in the HX sample series, parts of the cellulose fibril network were able to maintain their structure despite extensive hydrolysis and the relative amount of larger structures increased while the smaller structures were being hydrolysed. The slight decrease in the correlation length might be in connection with the increased power law exponents D (Table 2) and n (Table 3), which could be due to the hydrolysis of more thoroughly fibrillated segments of the network.

In the non-hydrolysed LX sample the peak in Fig. 5b was clearly located at smaller q values, as compared to the HX samples, and it seemingly shifted towards even lower q values during the hydrolysis. The location of the peak in the SANS intensity was directly reflected in the larger correlation length ξ of the LX and LX 25 % samples (28 and 38 nm, Table 3), compared to those of the HX samples. The correlation length of 28 nm in the non-hydrolysed LX sample was confirmed by the fit to the corresponding SAXS data, which covered also the intensities at lower

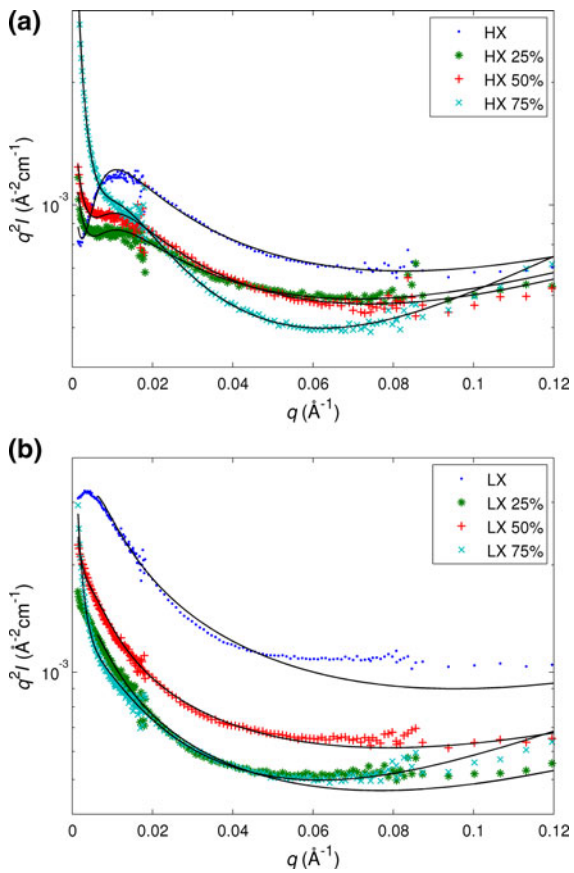

Fig. 5 Kratky plots of fits of Eq. 3 (*solid lines*) to SANS intensities of enzymatically hydrolysed NFC in 100 % D_2O: **a** NFC with original high xylan content (HX), **b** NFC prehydrolysed with xylanase, having low xylan content (LX)

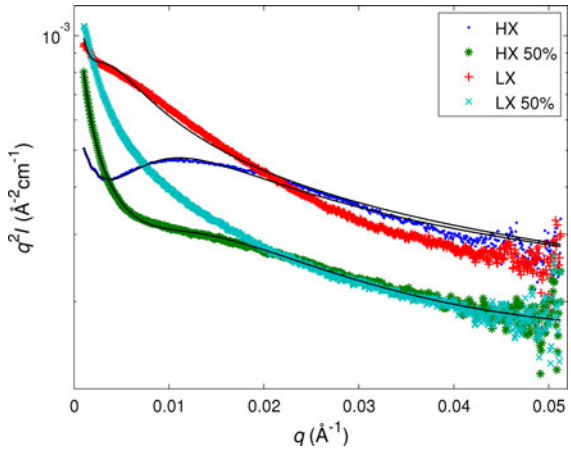

Fig. 6 Kratky plots of fits of Eq. 3 (*solid lines*) to SAXS intensities of enzymatically hydrolysed NFC: NFC with original high xylan content (HX) and NFC prehydrolysed with xylanase, having low xylan content (LX)

q values. It may be reasonable to assume that in the most hydrolysed LX 50 % and LX 75 % samples the peak observed in the other samples was located outside of the available q range, even though the fits of Eq. 3 to the whole data of these samples suggest smaller correlation lengths (18 and 13 nm with SANS). However, as for the HX series also, the power law scattering term (first term in Eq. 3) seemed to dominate over the correlation term (second term in Eq. 3) during later phases of hydrolysis and the contribution of the correlation term in the most hydrolysed samples was minor as compared to the power law term. The relative areal contribution of the second term in Eq. 3 to the fit was 0.08 and 0.09 for samples LX 50 % and LX 75 %. In addition to larger correlation lengths, the LX samples, in particular the less hydrolysed ones, showed a wide plateau in the Kratky plot between $q = 0.05$ and 0.15 Å^{-1} (partly visible in Fig. 5b), corresponding to Bragg distances between 4 and 13 nm. This feature very likely arose from the cross-sectional repeating distance of parallel elementary microfibrils, which is an indication of remaining microfibril aggregates in the LX and LX 25 % samples, suggesting a partly incomplete fibrillation of the NFC with lower xylan content.

Xylan content influencing the changes in structure during enzymatic hydrolysis

The hydrolysis of nanocellulose with higher (HX) and lower (LX) xylan proportion, 24 and 12 %, respectively, was clearly distinct, as observed with both SANS and SAXS. Without partially removing xylan prior to fibrillation (HX samples), the NFC network partly maintained its shape and structure up to 75 % hydrolysis. This was concluded based on the hardly changed correlation distance (Table 3) and the preserved location of the shoulder feature (Figs. 5a and 6, HX samples). The result is also in accordance with previous observations using wide-angle x-ray scattering (WAXS) and dynamic FT-IR spectroscopy (Penttilä et al. 2013). The preservation of lignocellulose ultrastructure could be attributed to the steric hindrance of hydrolysis by the location of xylan, which presumably protected cellulose fibrils against hydrolysis by covering their surface. As a consequence, the processive movement of cellulases on the surface of cellulose fibrils would be interrupted by xylan obstacles. However, the data obtained in this study is unable to provide unambiguous information on the exact location of xylan.

In the sample series prehydrolysed with xylanase prior to fibrillation (LX samples), the xylan still present in the samples seemed to have less obvious role in limiting the hydrolysis of cellulose. The xylan-to-glucan ratio in the hydrolysate of the LX series remained approximately constant implying that xylan was hydrolysed concomitantly with cellulose, but it also remained below that of the original substrate throughout the hydrolysis (Penttilä et al. 2013). Enzymatic hydrolysis weakened the correlation between the fibrils of the network as well as led to an increase in the interfibrillar distance. These results indicate a gradual disruption of the network in the absence of excess xylan.

Larger structures remaining despite enzymatic hydrolysis

The gradual increase in the low-q scattering during hydrolysis (Figs. 1 and 2) and the increase of the power law exponents (D in Table 2 and n in Table 3), especially during the later phases of the hydrolysis, indicate that the most recalcitrant fraction of the heterogeneous substrate contained larger structures. That is to say, irrespective of the xylan content, the hydrolysis was eventually limited by the recalcitrance of some larger particles present in the samples. These larger structures were not necessarily tight bundles of microfibrils, as those present in the less hydrolysed

samples of the low-xylan series, but they may have contained other kinds of structural features that were unfavourable of an efficient action of the different enzymes. One might speculate these to include features promoting the trapping of enzymes or preventing them from proceeding along the cellulose chains (Jalak and Väljamäe 2010; Murphy et al. 2012). Besides being present in the originally accessible parts of the substrate, structures hindering the enzymatic hydrolysis could be revealed during the hydrolysis, by for instance a more rapid hydrolysis of some parts of the substrate. It should also be emphasized that because the hydrolysis residues were measured in never-dried state, the possibility of structural artefacts caused by drying of the sample (Penttilä et al. 2010) was excluded. The gradual weakening of the interfibrillar correlation and the increased proportion of larger structures together imply that the enzymes were able to hydrolyse the most susceptible fibril segments completely, whereas the less susceptible segments and parts of the network remained. This led to an apparent selectivity of the hydrolysis.

Conclusions

In this work, small-angle scattering methods were applied to examine the changes occurring in the structure of nanofibrillated cellulose during enzymatic hydrolysis. Xylan was seen to protect the microfibrillar network and the hydrolysis of more thoroughly fibrillated segments of the network was described by increased mesh size and proportion of larger structures. Despite the extensive fibrillation of the raw material, the hydrolysis was eventually limited by the heterogeneity of the substrate. The segments of the polysaccharide network most susceptible to enzymatic hydrolysis were hydrolysed faster, leaving only larger, less susceptible fragments and explaining the apparent selectivity of the reaction.

Acknowledgments The authors thank University of Helsinki Research Funds, the Academy of Finland (2105059) and the Finnish Cultural Foundation for financial support. Jaakko Pere from VTT Technical Research Centre of Finland is thanked for providing the nanocellulose substrates for the hydrolysis.

References

Alvira P, Tomás-Pejó E, Ballesteros M, Negro MJ (2010) Pretreatment technologies for an efficient bioethanol production process based on enzymatic hydrolysis: a review. Bioresour Technol 101:4851–4861. doi:10.1016/j.biortech.2009.11.093

Arantes V, Saddler JN (2010) Access to cellulose limits the efficiency of enzymatic hydrolysis: the role of amorphogenesis. Biotechnol Biofuels 3:4. doi:10.1186/1754-6834-3-4

Bubner P, Dohr J, Plank H, Mayrhofer C, Nidetzky BJ (2012) Cellulases dig deep: in situ observation of the mesoscopic structural dynamics of enzymatic cellulose degradation. J Biol Chem 287:2759–2765. doi:10.1074/jbc.M111.257717

Chundawat SPS, Beckham GT, Himmel ME, Dale BE (2011) Deconstruction of lignocellulosic biomass to fuels and chemicals. Annu Rev Chem Biomol Eng 2:121–145. doi:10.1146/annurev-chembioeng-061010-114205

Hallac BB, Ragauskas AJ (2011) Analyzing cellulose degree of polymerization and its relevancy to cellulosic ethanol. Biofuels Bioprod Biorefin 5:215–225. doi:10.1002/bbb.269

Horkay F, Hammouda B (2008) Small-angle neutron scattering from typical synthetic and biopolymer solutions. Colloid Polym Sci 286:611–620. doi:10.1007/s00396-008-1849-3

Igarashi K, Uchihashi T, Koivula A, Wada M, Kimura S, Okamoto T, Penttilä M, Ando T, Samejima M (2011) Traffic jams reduce hydrolytic efficiency of cellulase on cellulose surface. Science 333:1279–1282. doi:10.1126/science.1208386

Jalak J, Väljamäe P (2010) Mechanism of initial rapid rate retardation in cellobiohydrolase catalyzed cellulose hydrolysis. Biotechnol Bioeng 106:871–883. doi:10.1002/bit.22779

Kennedy CJ, Cameron GJ, Šturcová A, Apperley DC, Altaner C, Wess TJ, Jarvis MC (2007) Microfibril diameter in celery collenchyma cellulose: X-ray scattering and NMR evidence. Cellulose 14:235–246. doi:10.1007/s10570-007-9116-1

Kent MS, Cheng G, Murton JK, Carles EL, Dibble DC, Zendejas F, Rodriquez MA, Tran H, Holmes B, Simmons BA, Knierim B, Auer M, Banuelos JL, Urquidi J, Hjelm RP (2010) Study of enzymatic digestion of cellulose by small angle neutron scattering. Biomacromolecules 11:357–368. doi:10.1021/bm9008952

Leppänen K, Andersson S, Torkkeli M, Knaapila M, Kotelnikova N, Serimaa R (2009) Structure of cellulose and microcrystalline cellulose from various wood species, cotton and flax studied by X-ray scattering. Cellulose 16:999–1015. doi:10.1007/s10570-009-9298-9

Lindner P (2002) Scattering experiments: experimental aspects, initial data reduction and absolute calibration. In: Lindner P, Zemb T (eds) Neutrons, x-rays and light: scattering methods applied to soft condensed matter. Elsevier, Amsterdam, pp 23–48

Lopez-Rubio A, Gilbert EP (2009) Neutron scattering: a natural tool for food science and technology research. Trends Food Sci Technol 20:576–586. doi:10.1016/j.tifs.2009.07.008

Murphy L, Cruys-Bagger N, Damgaard HD, Baumann MJ, Olsen SN, Borch K, Lassen SF, Sweeney M, Tatsumi H, Westh P (2012) Origin of initial burst in activity for Trichoderma reesei endo-glucanases hydrolyzing insoluble cellulose. J Biol Chem 287:1252–1260. doi:10.1074/jbc.M111.276485

Penttilä PA, Várnai A, Leppänen K, Peura M, Kallonen A, Jääskeläinen P, Lucenius J, Ruokolainen J, Siika-aho M,

Viikari L, Serimaa R (2010) Changes in submicrometer structure of enzymatically hydrolyzed microcrystalline cellulose. Biomacromolecules 11:1111–1117. doi:10.1021/bm1001119

Penttilä PA, Várnai A, Pere J, Tammelin T, Salmén L, Siika-aho M, Viikari L, Serimaa R (2013) Xylan as limiting factor in enzymatic hydrolysis of nanocellulose. Bioresour Technol 129:135–141. doi:10.1016/j.biortech.2012.11.017

Santa-Maria M, Jeoh T (2010) Molecular-scale investigations of cellulose microstructure during enzymatic hydrolysis. Biomacromolecules 11:2000–2007. doi:10.1021/bm100366h

Shibayama M (2011) Small-angle neutron scattering on polymer gels: phase behavior, inhomogeneities and deformation mechanisms. Polym J 43:18–34. doi:10.1038/pj.2010.110

Wang L, Zhang Y, Gao P, Shi D, Liu H, Gao H (2006) Changes in the structural properties and rate of hydrolysis of cotton fibers during extended enzymatic hydrolysis. Biotechnol Bioeng 93:443–456. doi:10.1002/bit.20730

Waters DJ, Engberg K, Parke-Houben R, Ta CN, Jackson AJ, Toney MF, Frank CW (2011) Structure and mechanism of strength enhancement in interpenetrating polymer network hydrogels. Macromolecules 44:5776–5787. doi:10.1021/ma200693e

Zhou W, Schüttler H-B, Hao Z, Xu Y (2009) Cellulose hydrolysis in evolving substrate morphologies I: a general modeling formalism. Biotechnol Bioeng 104:261–274. doi:10.1002/bit.22389

Zhu L, O'Dwyer JP, Chang VS, Granda CB, Holtzapple MT (2008) Structural features affecting biomass enzymatic digestibility. Bioresour Technol 99:3817–3828. doi:10.1016/j.biortech.2007.07.033